Journal of Hydrology: Regional Studies 55 (2024) 101922

Contents lists available at ScienceDirect

Journal of Hydrology: Regional Studies

journal homepage: www.elsevier.com/locate/ejrh

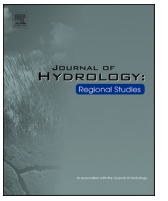

Climate variability and hydrology impacts in east Africa's Rwenzori Mountains

Mark R. Jury [a,b]

[a] Physics Dept, University of Puerto Rico Mayagüez, 00681, Puerto Rico
[b] Geography Dept, University of Zululand, KwaDlangezwa 3886, South Africa

ARTICLE INFO

Keywords:
African Rift Valley
Rwenzori Mountains
Climate variability
Declining streamflow

ABSTRACT

Study region: The eastern flank of the 4 km Rwenzori Mountains and the Mobuku catchment 0.25–0.4 N, 29.85–30.1E are the geographic area for detailed analysis.
Research focus: Hydro-climate variability is studied using high resolution satellite- and model-assimilated products in the period 1980–2023. The Mobuku catchment receives rainfall of 3–6 mm/day which generates an eastward discharge of 100 m^3/s that declines rapidly downstream, thereby limiting hydro-power availability.
New insights: Long-term trends in cloud fraction and potential evaporation reveal a tendency for drying associated with increasing easterly winds, subsidence near the mountain top, and warming of +.04 C/year that is melting glaciers. These constrain runoff on the eastern flank of the Rwenzori Mountains. Low river flows in Dec-Mar correspond with dry air intrusions from the northeast. High river flows in Jul-Nov are modulated by sea temperatures in the Indian Ocean that oscillate east-west at ~3 year interval. Improved understanding of climate variability will contribute to better management of Uganda's hydro-power resources.

1. Introduction

The Rwenzori Mountains tower 4000 m above east Africa's Rift Valley. Orographic rainfall amidst the semi-arid savanna creates sharp climatic gradients. Dry northeast and southeast airflow from the Indian Ocean in January and July alternates with humid westerlies from the Congo in April and October (Hogan et al., 2015; Yang et al., 2015; Jury 2017a,b; Nicholson, 2018) generating over one meter of rainfall annually. Year-to-year variability of east Africa's climate is modulated by the Pacific El Niño–Southern Oscillation (ENSO) and Indian Ocean Dipole (IOD). Palmer et al. (2023) describe how the warming of east Pacific and west Indian Ocean sea temperatures are linked to a zonal wind circulation (Walker Cell) that stimulates moist convection in the equatorial trough over east Africa. The ENSO and IOD tend to act collectively to produce cycles of drought and flood but can weaken or shift out-of-phase leaving neutral conditions. In 2020 tropical downpours raised Rift Valley lake levels over 20 % (Herrnegger et al., 2021).

Nsubuga et al. (2014) provide a review of water resources in Uganda. They note that many catchments draining into the Rift Valley conduct little runoff to the White Nile. The warm dry lowlands to the east of the Rwenzori Mountains act like a sponge, while the mountain tops exhibit rapid warming (Thompson et al., 2006; Pepin et al., 2015; Prinz et al., 2018; MacKay et al., 2021). Although rainfall trends are small, greater evaporation has consequences for discharge (Taylor et al., 2009). Deforestation smoke plumes spread across central Africa and aggravate climate change by amplifying thermal stability and the annual cycle (Jury and Whitehall, 2010; UNDP, 2013; Clarke et al., 2022), eg. drier dry / wetter wet seasons.

E-mail address: mark.jury@upr.edu.

https://doi.org/10.1016/j.ejrh.2024.101922
Received 16 April 2024; Received in revised form 26 July 2024; Accepted 28 July 2024
Available online 5 August 2024

Eighty percent of Uganda's installed electrical generating capacity is hydropower and its river flows are adversely affected by drought, degraded catchment landscapes and increased siltation. Discharge to the Bugoye hydropower plant (0.3 N, 30.1E) has declined in recent decades (Berkley Energy, 2023). Modelling studies have identified how the balance between rainfall and potential evaporation alters infiltration and runoff as the Mobuku River decends from 4000 m to 1000 m elevation. Low flows have prevailed since 2011, interspersed with flash-flood events in May 2013, May 2020 and Mar 2023. A short record of rain gauge measurements at Kasese in the Rift Valley indicate that dry spells occur ~ 6 % of the time (Byakatonda et al., 2021).

Here the objective is to study the hydro-climate of the eastern Rwenzori Mountains via gauge- satellite- model- assimilated data, to analyze short- and long-term variability of discharge, and to understand the causes of abnormal runoff via statistical analysis, seasonal composites and case studies. Validation of data assimilation products could not be done because of insufficient measurements in the upper catchment.

2. Data analysis

Meteorological parameters that quantify the hydro-climate include: ERA5 European Reanalysis dewpoint temperature, potential evaporation, air temperature, humidity, and wind fields. Meteosat cloud fraction and EC (European Community) river discharge were obtained. Rainfall measurements derive from CHIRP (Meteosat IR) and GPM satellite, CHIRPS2 gauge, and ERA5 model hindcast. These products have a spatial resolution ~25 km and temporal extent 1980–2023 except GPM 2000+. Modis satellite vegetation fraction (NDVI) and IR land surface temperature at 1 km resolution were analyzed for landscape changes since 2000.

Daily and monthly time series (Appendix A1a,b) were extracted for the eastern Rwenzori: 0.25–0.4 N, 29.85–30.1E. Mean annual cycles, histograms, and temporal correlations were calculated 1980–2023 for local hydro-climate variables and sea temperatures representing the IOD. After smoothing with an 18-month polynomial filter to remove seasonal cycles, the 528-month time series were analyzed for linear trends by least squares regression. Statistical significance with ~ 45 degrees of freedom requires a product-moment coefficient $r > |0.25|$ for 95 % confidence.

To understand hydro-climate fluctuations, daily and monthly time series were ranked for dry and wet spells. Short-term events in Feb 2012 and Apr 2016 were analyzed via satellite net OLR (outgoing longwave radiation), low level wind fields and back-trajectories. Point-to-field statistics were computed to relate rainy spells to westerly winds from the Congo. Zonal circulations were analyzed for warming and drying trends, and seasonal composite meridional circulations and humidity anomalies were studied. The diurnal cycle of 3-hourly satellite rainfall and wind was analyzed to understand how afternoon thunderstorms are spawned west of the Rift Valley. Rainfall projections for the Mobuku catchment utilized the CNRM6 ssp585 simulation 1980–2050, due to its 50 km resolution and ability to reflect diurnal and orographic signals (Voldoire et al., 2019).

The research is constrained by sparse weather observations around the Rwenzori Mountains (Appendix A1c), and relies on model-interpolated satellite measurements for insights on the local climate. Table 1 lists the datasets, acronyms and documentation below. Without hydrological information in the upper catchment, validations could not be attempted. This poses a limitation in the study, and means that statistical analysis of past observations is restricted to the satellite era - to improve confidence in scientific interpretations.

3. Results

3.1. Climate and Geography: spatial analysis

Equatorial east Africa experiences a bimodal climate with wet spells in Mar-May and Sep-Nov. Low-level winds sweep inland from the northeast in Dec-Feb and from the southeast in Jun-Aug (Fig. 1a,b). Despite passing over warm seas, this divergent airflow is relatively dry due to atmospheric subsidence. The study area topography (Fig. 1c) reflects the Rwenzori Mountains towering above the SW-NE oriented Rift Valley. The steep slopes naturally generate runoff that infiltrates along the way, providing geographic context for the research.

Table 1
Characteristics of datasets employed: acronyms, variables, resolution and reference.

Acronym	Name (variables)	Horz.Res.	Reference Document
CHIRPS2	Climate Hazards interpolated gauge v2 (precipitation)	5–25 km	Funk et al. (2014)
CloudSAT	Satellite microwave radar (reflectivity)	1 km	Tanelli et al. (2008)
CNRM6	Centre National Rech. Meteo. coupled ensemble model v6 (rainfall)	50 km	Voldoire et al. (2019)
EC	European Community reanalysis (discharge)	20 km	Harrigan et al. (2020)
ERA5	European Reanalysis v5 (air & dewpt temp, humidity, pot. evap, wind, vertical motion)	25 km	Hersbach et al. (2020)
GPM	Global Precipitation Monitoring (multi-satellite rainfall)	20 km	Hou et al. (2014)
Meteosat	European Space Agency satellite (cloud fraction, IR cold cloud duration)	5–25 km	Karlsson et al. (2020)
MERRA2	Modern era reanalysis for research & applications v2 (diurnal cycle)	50 km	Gelaro et al. (2017)
MODIS	Moderate imaging sensor (satellite VIS vegetation and IR land temperature)	1 km	Pinzon and Tucker, (2014)
net OLR	Satellite net outgoing longwave radiation (cloud convection)	100 km	Lee et al. (2007)

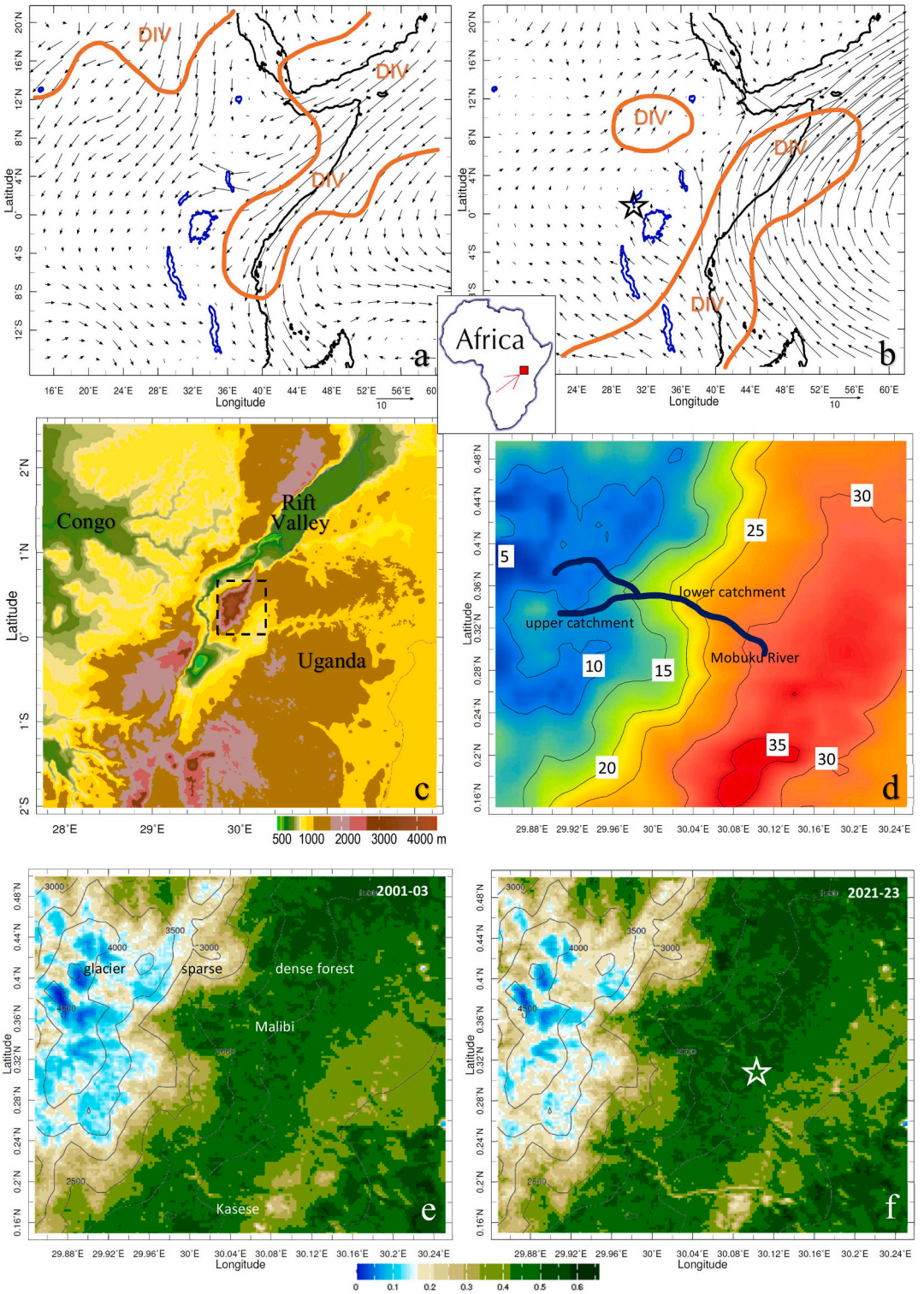

Fig. 1. a) Average January circulation (vector key), b) same in July, in the 1–2 km layer reflecting airflow divergence (contour $> 3\ 10^{-6}\ s^{-1}$) from the coastal monsoon. c) Topographic map and study area (dashed). d) Satellite IR 2001–2023 mean day-time land surface temperature (°C). e,f) Modis satellite vegetation fraction over the Rift Valley and snow-capped Rwenzori mountains: b) 2001–03 before and c) 2021–23 now. Star is the Bugoye hydropower plant in b, f), Mobuku River is dark blue line in d); scales vary.

The 2001–2023 average Modis satellite infrared (IR) day-time land surface temperature (Fig. 1d) shows values of ~ 5 C at the highest point of the Rwenzori. An isotherm indicating values < 10 C encircle the retreating glaciers. In contrast, Rift Valley surface temperatures exceed 35 C; thus sharp hydro-climate gradients exist along the eastern flank facing Uganda. The Modis vegetation maps in 2001–03 and 2021–23 (Fig. 1e,f) indicate a spread of dense forests to higher elevation that may alter the ratio of runoff to infiltration. The river channels show declining vegetation cover in the recent period due to increased traffic and urbanization (Malibi,

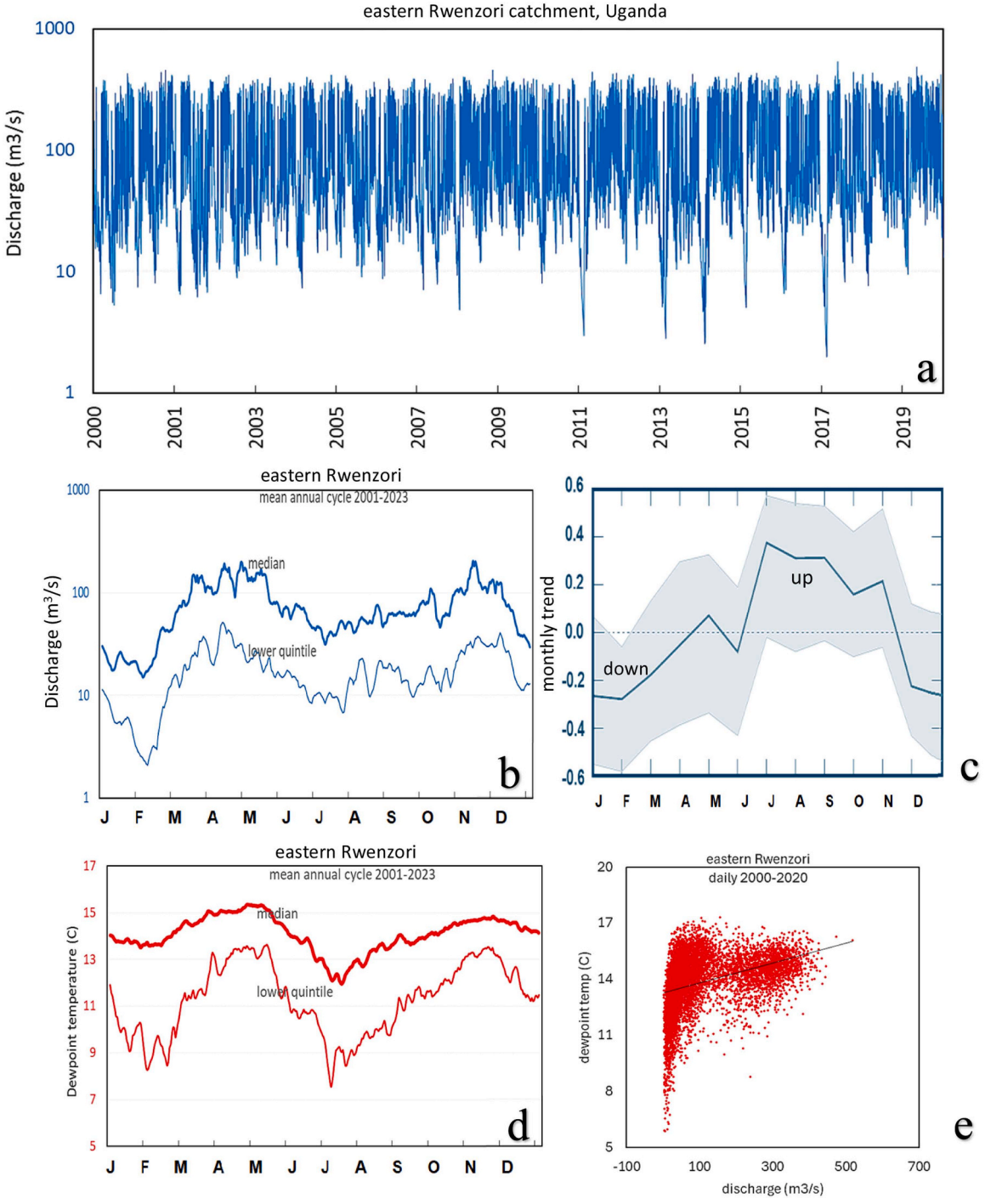

Fig. 2. a) Daily time series of EC discharge of the Mobuku River 2000–2020 (log scale), b) Annual cycle of discharge median and lower quintile. c) Correlation of linear trend in EC discharge for each month since 1979. d) Annual cycle of dewpoint temperature median and lower quintile. e) Scatterplot of daily dewpoint temp vs river discharge, highlighting two regimes.

Kasese). The spatial patterns are expressed in temporal context below.

3.2. Hydro-climate: temporal analysis

The EC daily river discharge 2000–2020 is presented in Fig. 2a and reflects a catchment average ~ 100 m^3/s. Values often decline below 10 m^3/s during Jan-Feb, insufficient for downstream hydropower generation. Peak discharge was on 20 May 2018 (518 m^3/s). The mean annual cycle (Fig. 2b) alternates twice-yearly between 50 and 150 m^3/s. Trends in discharge each month reveal growing seasonality (Fig. 2c): down-trends in Dec-Mar / up-trends in Jul-Nov, indicative of less / more runoff during the northeast / southeast monsoon. The frequency of low flow at the Bugoye hydropower plant 0.3 N, 30.1E increased from 2 % to 5 % after 2011. This appears

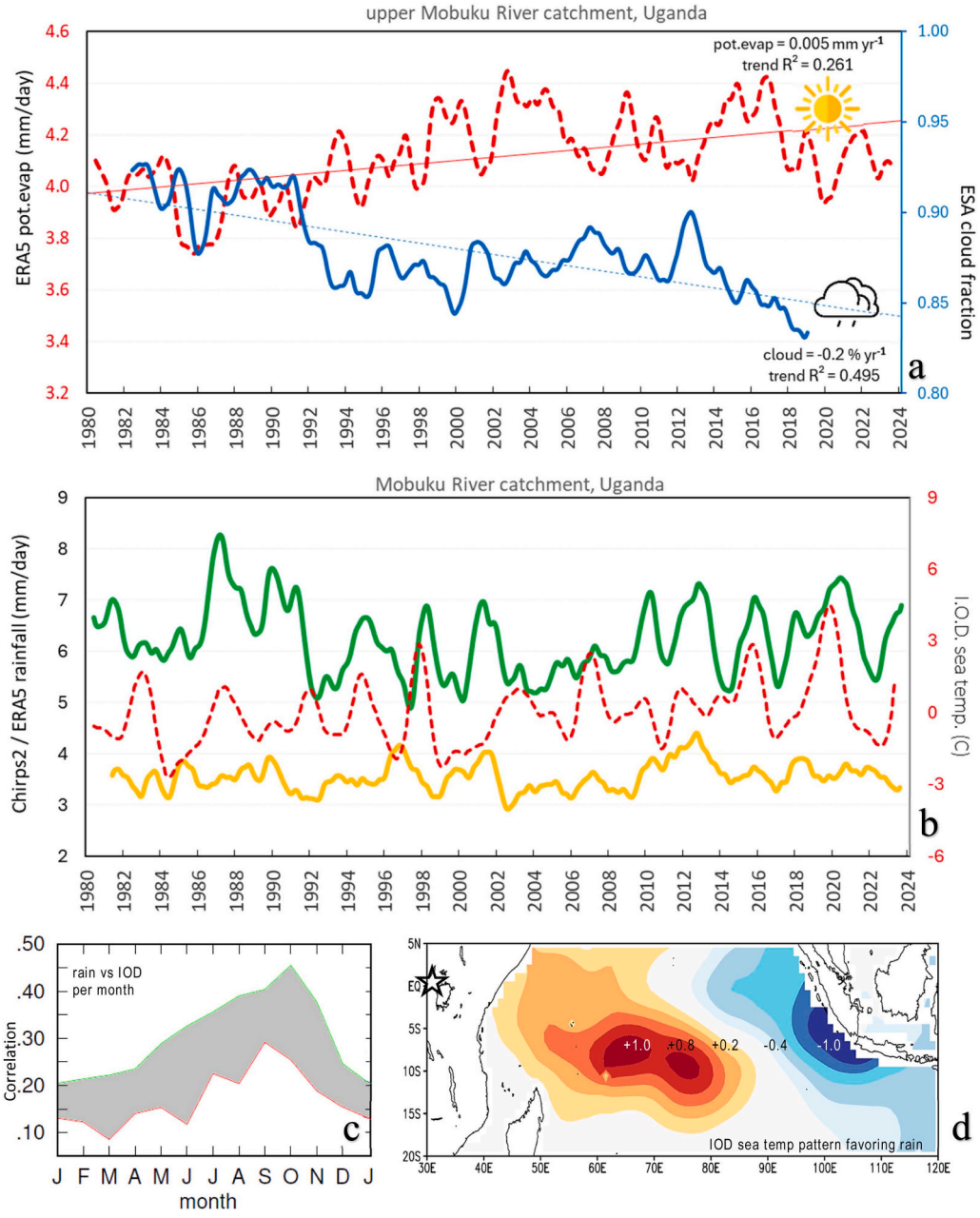

Fig. 3. a) Time series of 18-month smoothed potential evaporation and Meteosat cloud fraction with trends. b) Smoothed time series of rainfall in the upper (green) and lower (gold) catchment from ERA5 and Chirps2 respectively; Indian Ocean Dipole (IOD) sea temperature is red dashed. c) Correlation of upper catchment rainfall with IOD per month 1980–2023 (mean r-value red line, upper tercile green), d) IOD sea temperature pattern (standardized departures +red –blue).

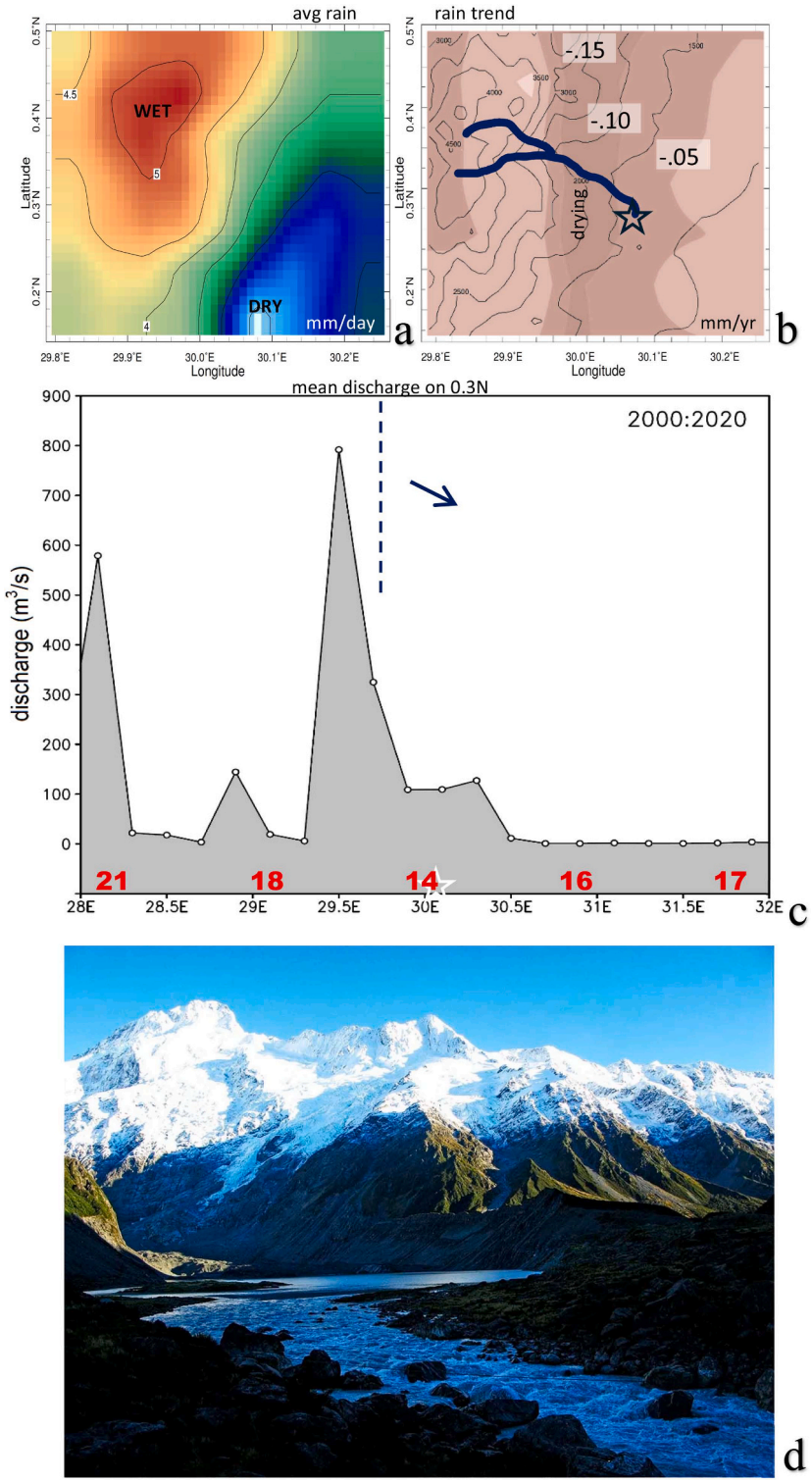

Fig. 4. Maps of Meteosat IR CCD estimated: a) average rainfall (mm/day) and b) linear trend (shaded mm/yr) 1981–2023 with river channel and elevation contours. c) Average EC discharge from 28 to 32E along 0.3 N with dashed line dividing the watershed runoff (arrow), dewpoint temp. = red numbers, scales vary. d) Photograph of the Mobuku River flowing out of the snow-capped Rwenzori Mountains in the 1970s (credit: Sierra Intl).

to be related to changes in the runoff – infiltration ratio.

Dewpoint temperature (Td) is a useful metric that reflects the modulation of both rainfall and evaporation. Its mean annual cycle (Fig. 2d) shows a bi-modal climate with dry spells in February and July, when Td dips below 10 C. The scatterplot of daily Td and river discharge (Fig. 2e) correlates simultaneously r =0.36 and concentrates in two regimes of low and high flow. Lag-correlations are no better, and indicate that the cascading effect of moist air convergence, convective clouds, rainfall and finally runoff - is quick.

The time series of 18-month filtered ERA5 potential evaporation (Fig. 3a) reflects values above 4 mm/day, and a rising trend of.005 mm/yr with r^2 =0.26. In conjunction, Meteosat cloud fraction over the eastern flank of the Rwenzori has declined from 90 % to 85 %, a significant down-trend of 0.2 % yr^{-1} with r^2 =0.49. The 18-month filtered rainfall time series are presented in Fig. 3b for the upper and lower catchment, using ERA5 reanalysis and CHIRPS2 gauge products respectively. Rainfall in the highlands is double the lowlands (~ 6 vs 3 mm/day). Neither rainfall time series has a significant trend. ERA5 has a wet bias in Dec-Mar season compared with CHIRPS2, in other months there is consensus. Runoff increases during positive IOD sea temperatures (Fig. 3c,d) which describe a warm-west pattern affecting the Jul-Nov months (Roy et al., 2024). Hence low runoff tends to happen during negative IOD (cool-west sea temp). The IOD is underpinned by a slowly tilting upper ocean thermocline (see-saw) in conjunction with Pacific El Nino (Jury, 2018). The IOD index leads Mobuku catchment rainfall by ~3 months (r =0.30), a weak correlation that may related to insensitivity of the Congo monsoon to conditions in the Indian Ocean (Cook and Vizy, 2019; MacLeod et al., 2024).

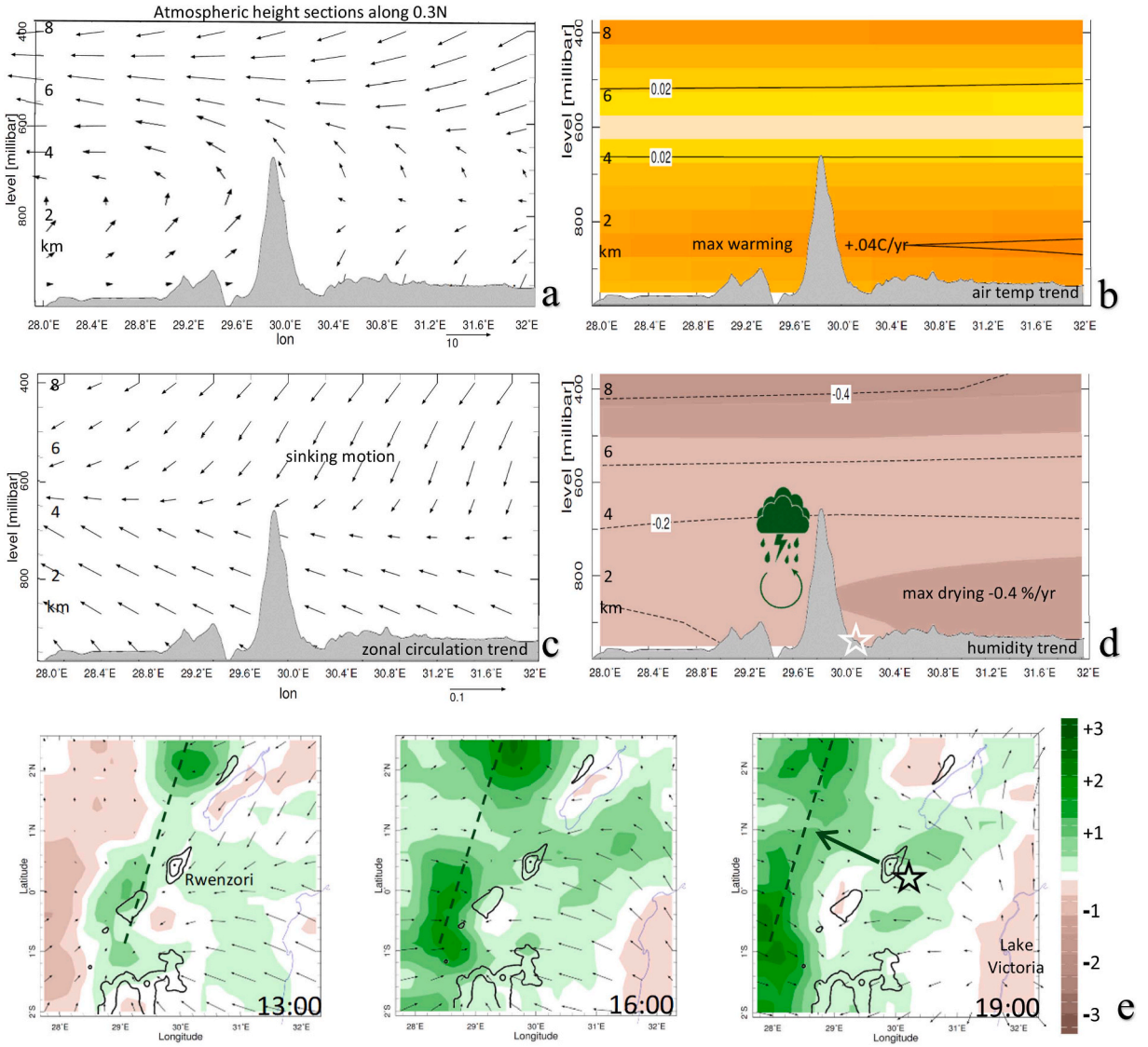

Fig. 5. 1981–2023 atmospheric height sections from 28 to 32E along 0.3 N of: a) mean zonal circulation, b) air temperature trend (C/yr), c) zonal circulation trend (m s^{-1}/yr), d) humidity trend (% yr^{-1}); conceptual wind rotor and cloud icons over the western flank. e) Left-right sequence of diurnal anomalies of 3 hourly satellite rainfall (shaded mm/hr) and near-surface wind (max vector 3 m/s) at 13, 16, 19 hr, illustrating the 'afternoon wave' (Aug-Oct season); topographic contours > 2000 m. Note that b,d) are shaded and contoured.

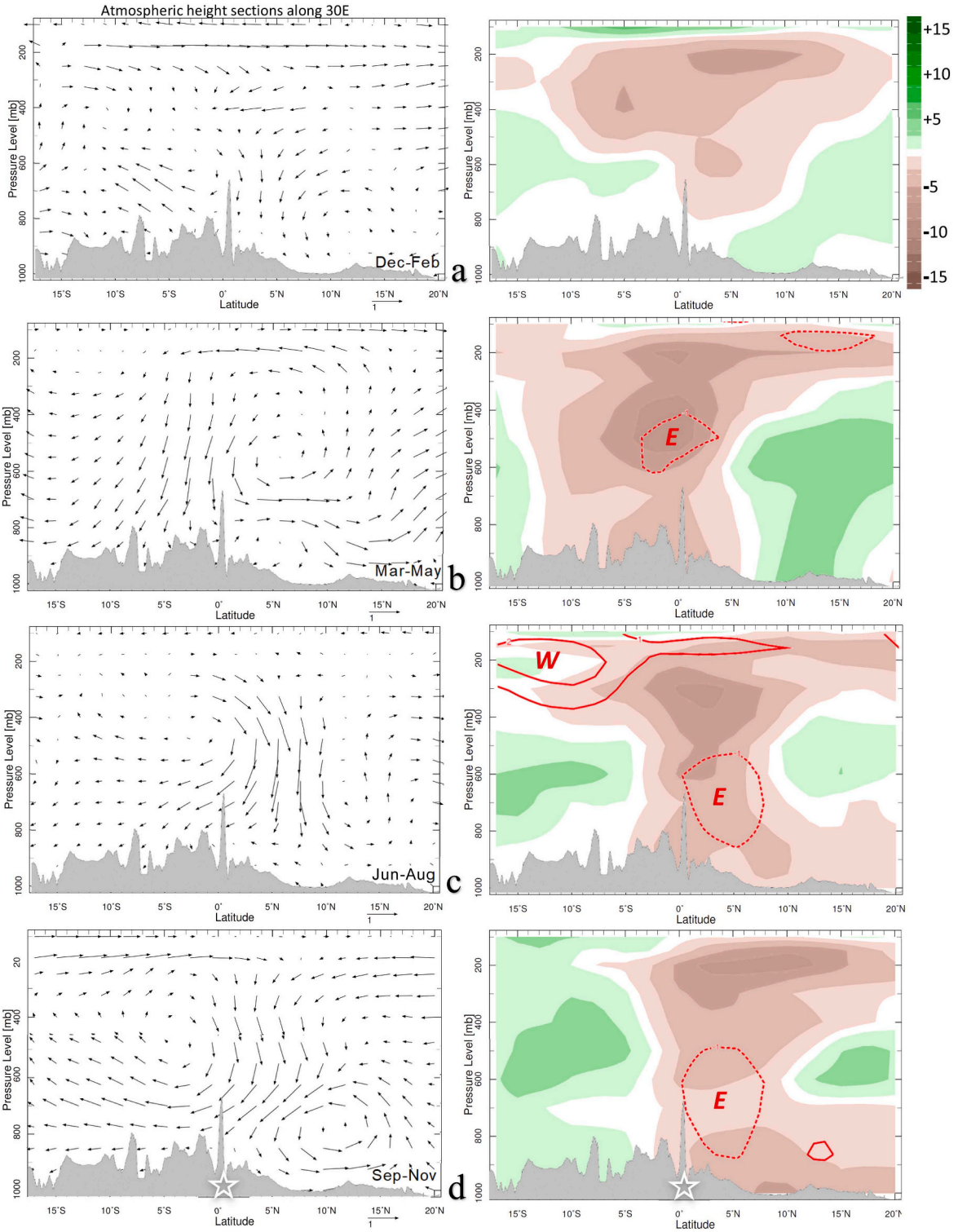

Fig. 6. Latitude - height section of (left column) vector Hadley circulation anomalies, and (right column) humidity anomalies (scale in a) and red dashed zonal wind anomalies for top-10 composite dry seasons: a) Dec-Feb, b) Mar-May, c) Jun-Aug, d) Sep-Nov. The symbol ***E*** = dry airflow from the east.

In the following section, long-term trends in rainfall and the atmospheric circulation are studied and linked via composite and diurnal analyses.

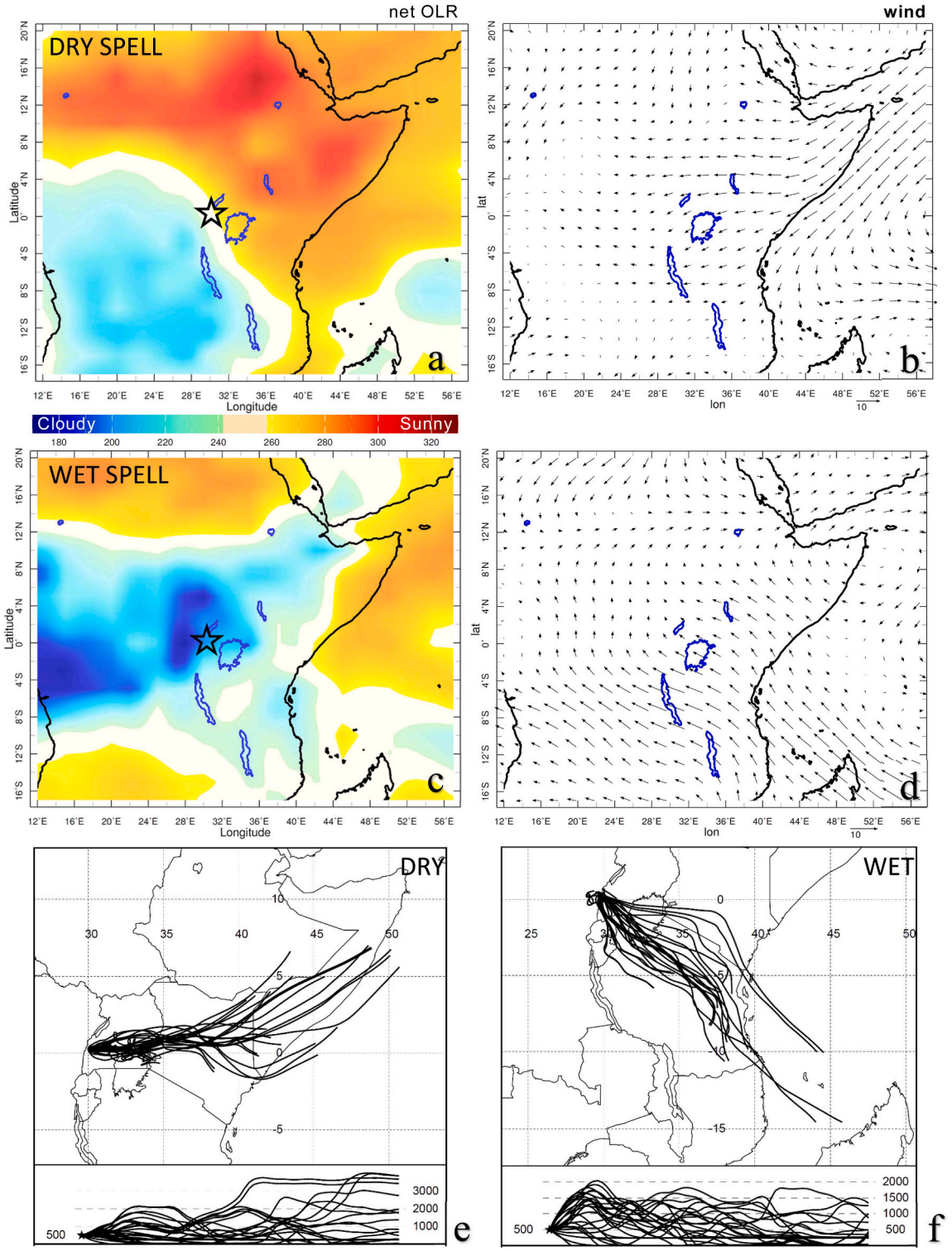

Fig. 7. Satellite net OLR field (W/m^2) and (right) 850 hPa wind (max 10 m/s) during: a,b) a dry spell 1–10 Feb 2012 (upper) with discharge < 3 m^3/s and c,d) a wet spell 9–18 Apr 2016 with discharge > 300 m^3/s. e,f) Comparison of backward trajectories in the dry (left) and wet spell, in map view and height section (lower).

3.3. Rainfall pattern and trend

Fig. 4a,b illustrates the mean pattern and linear trend of Meteosat IR-CCD rainfall 1981–2023. The average value exceeds 5 mm/day over the Rwenzori highlands but is halved in the Rift Valley. There is a zone of downward trend (-0.10 mm/yr) along the 2000 m elevation, consistent with reduced cloud fraction and rising potential evaporation (cf. Fig. 3a).

Zonal gradients in mean river discharge on 0.3 N latitude (Fig. 4c) exhibit a peak ~ 800 m^3/s on the western flank of the Rwenzori

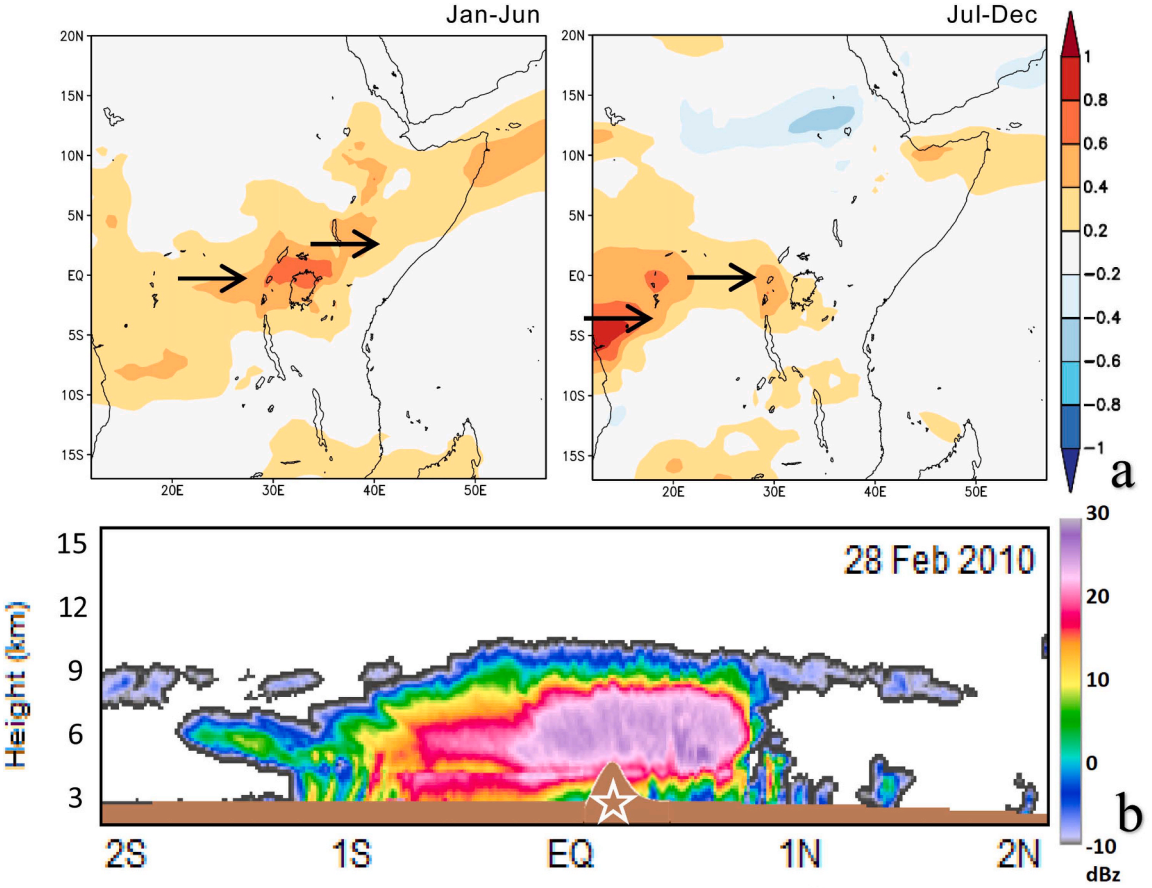

mon	day	rain	run	disc
Feb	27	2.8	1.1	62
Feb	28	10.7	2.2	54
Mar	1	8.1	14.0	62
Mar	2	1.8	0.1	53
Mar	3	1.1	0.8	230

c

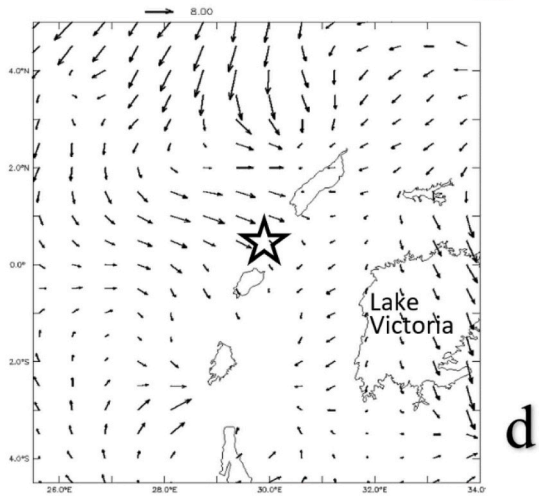

Fig. 8. a) Regression of eastern Rwenzori rainfall onto 700 hPa zonal wind field 1980–2023 first and second half of year, Congo westerlies - red shaded (mm day^{-1}/m s^{-1}). b) Latitude-height section of satellite cloud reflectivity along 30E longitude on 28 Feb 2010, c) data table of unseasonal runoff (mm/day, m^3/s). d) 850 hPa wind map 14:00 28 Feb 2010 showing westerly intrusion from the Congo.

(29.5E). Discharge on the eastern flank declines to ~10 m^3/s in the Rift Valley (30.5E) due to warm weather and soil infiltration. Snow over the Rwenzori (Fig. 4d) is infrequent and delivered by sub-tropical cold fronts from the south (Apr-Jun) or from the north (Oct-Dec). Snow cover above 3000 m is < 1 % most of the time, because cold air outbreaks over tropical Africa tend to be dry. During the satellite era, mountain top snow events (reaching 8 % coverage) were noted in Nov 1982, Jun 1985, Apr 2018 and Nov 2019.

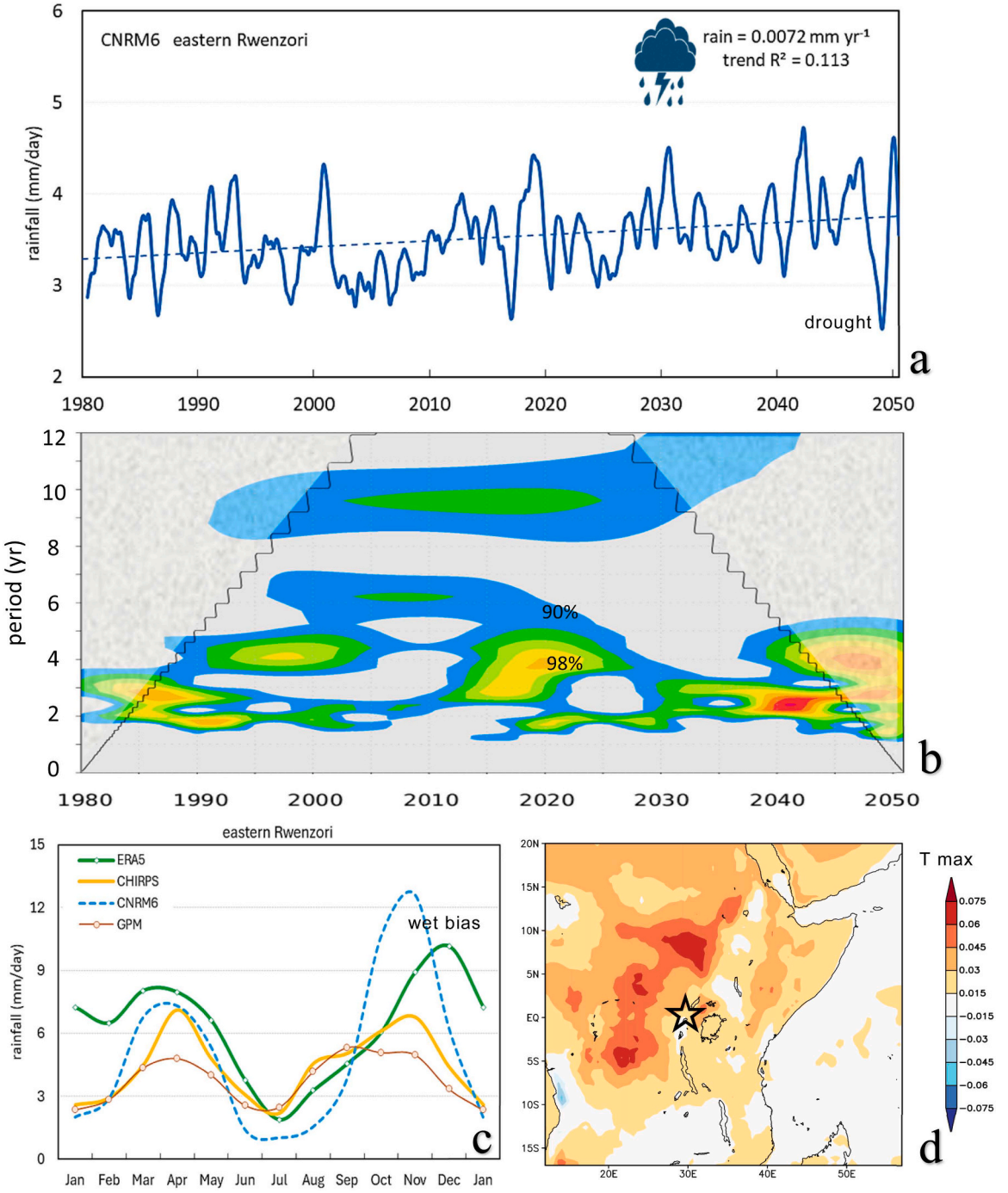

Fig. 9. a) CNRM6 model-projected 18-month filtered catchment rainfall, and b) its wavelet spectral energy shaded from 90 % to 99 % confidence from blue to red. c) Inter-comparison of rainfall mean annual cycle, and d) trend of maximum air temperature 1980–2023 (C/yr).

3.4. Zonal circulation, gradients, and afternoon rain

Fig. 5a-d illustrates the zonal circulation and its trend in the context of changing temperature and humidity along a height section from 28 to 32E on 0.3 N latitude. Prevailing winds are from the east and show a tendency to accelerate in the lower levels (1980–2023). Subsidence is evident above 600 hPa (mountain top) which induces rapid warming.04 C/yr and drying in the 1.5 km layer (850 hPa) especially to the east. We conceptualize a lee-side rotor that sustains rainfall on the Congo side (Fig. 5d).

The mean diurnal rainfall and 850 hPa wind are analyzed for Aug-Oct season in Fig. 5e, focusing on temporal evolution during the afternoon. A SW-NE line of convection forms at 13:00 hr over the Rift Valley supported by easterly winds. The line of thunderstorms propagate slowly westward from 16:00–19:00 hr, moving from the Rwenzori Mountains into the Congo Basin, similar to Raghavendra et al. (2022). Evening rainfall continues over the eastern flank of the Rwenzori supported by airflow diverging from Lake Victoria. We see this as part of the larger push-pull of Congo and Indian airmasses by continental scale land- sea-breezes.

3.5. Hadley circulation

In Fig. 6a-d latitude-height sections on 30E longitude are analyzed to determine how the meridional Hadley Cell is involved in dry spells. Using a top-10 dry composite, there is a confused pattern in Dec-Feb with negative humidity anomalies in the upper troposphere. However in other seasons the Hadley Cell delivers subsidence in conjunction with easterly wind anomalies around 600 hPa (mountain top). Dry conditions over equatorial Africa are bracketed by wet sub-tropics, wherein the equatorial forms over the White Nile (10–15 N) in Mar-May. In Jun-Aug the southern sub-tropical jet (200 hPa, 10–15 S) imparts anticyclonic vorticity and low humidity over the Rwenzori. Hadley Cell subsidence is driven by a single overturning circulation rotor from the north in Mar-May and from the south in Jun-Aug, while in Sep-Nov a dual rotor emerges.

3.6. Short-term weather forcing

Ranking days with low and high discharge in the eastern Rwenzori catchment, dry and wet spell satellite net OLR and 850 hPa winds are analyzed in Fig 7a-d. In 1–10 Feb 2012 a northeast monsoon of 10 m/s induced sunny skies with OLR >300 W/m^2. Cloud development (low values of net OLR) was confined west of Lake Tanganyika and discharge east of the Rwenzori declined <3 m^3/s. In contrast, the 9–18 Apr 2016 wet spell saw southeasterly airflow of 10 m/s from Madagascar. The winds slowed along a SW-NE axis generating moist convection and net OLR <200 W/m^2. EC discharge in the Mobuku River rose above 300 m^3/s sustaining hydropower. Back-trajectories for airflow arriving over the catchment (Fig 7e,f) reveal contrasts in the sources of dry (Feb 2012, Kenya) and humid weather (Apr 2016, Tanzania).

The influence of moist airflow from the Congo is analyzed by point-to-field regression of Mobuku catchment rainfall onto 700 hPa zonal wind in Jan-Jun and Jul-Dec (Fig. 8a). In the 1st half year the westerly signal spreads toward the Indian Ocean indicating that a weakened northeast monsoon supports more rainfall. In the 2nd half year the westerly signal spreads toward the Atlantic Ocean.

A latitude-height section along 30E of satellite cloud reflectivity on 28 Feb 2010 (Fig. 8b) exhibits values >20 dBz above the Rwenzori Mountains. Data show a cascade of rainfall-runoff-discharge over a 3 day period (Fig. 8c), generating an estimated water volume of three billion litres. Westerly winds from the Congo are conspicuous (Fig. 8d) and shift moist convection to the eastern flank of the Rwenzori, as noted by Finney et al. (2020).

In the following section we shift focus from past observations to coupled model projections. Although these outputs have been validated over Africa (Munday and Washington, 2018), model ability to replicate sharp orographic gradients is limited.

3.7. Climate projection and model bias

CNRM6 projected rainfall for the eastern Rwenzori (Fig. 9a) under 5 W/m^2 radiative forcing, suggests a rising trend attributable to a faster Hadley circulation driving more equatorial and less subtropical rainfall (Wainwright et al., 2019; IPCC, 2021). Three year cycling (Fig. 9b) reflects the IOD see-saw. Dry spells in the Rwenzori are projected to be intense in association with accelerated easterlies and mid-level subsidence (cf. Fig. 5c). The historical mean annual cycle (Fig. 9c) follows the expected bi-modal pattern but reveals a wet bias for CNRM6 and ERA5 in Nov-Jan. The onset of the dry season is delayed in those products. In tracing this issue, many cases were found with anomalous orographic rainfall during wet spells associated with rapidly decelerating northeast winds.

Differential land-sea warming affects the regional climate. Over 1980–2023 maximum temperatures have increased +.05 C/yr inland (Fig. 9d) and draw airflow toward the Rift Valley. Afternoon winds depend on $\Delta U = gH/T\ (dT/dx)\ dt$, where H is surface layer, T temperature, dx distance, dt time (Pielke and Segal, 1986). A scale analysis yields: 10 m/s^2(100 m)/300 K (5/10^5 K/m) 5 10^4 s. An 8 m/s easterly wind is similated which moves upslope while diverging from the longshore monsoon. When the IOD is in cool/west phase, the dT/dx and divergence intensify, resulting in subsidence and desiccation.

4. Summary

This study employed hydro-climate data assimilation and coupled model simulation products to analyze the Mobuku catchment 0.25–0.4 N, 29.85–30.1E on the eastern flank of the Rwenzori Mountains. The analysis showed little trend in CHIRPS2 and ERA5 rainfall, whereas significant drying trends were observed in Meteosat cloud fraction and potential evaporation. This was linked (via height sections) to accelerating dry easterly winds and subsidence near the mountain top, contributing to a warming trend of +0.04 C/

yr and the melting of glaciers. The landscape of the upper catchment is sensitive to climate change: forests are spreading to higher elevation and retaining runoff which leads to downstream constraints on water resources and hydropower generation.

Analysis of the EC discharge record revealed multi-week spells of flow below 10 m^3/s in January-February associated with a trend of growing seasonality characterized by drier conditions from December to March and wetter conditions from July to November. Dry spells tend to occur during the cold-west Indian Ocean Dipole (IOD) sea temperature pattern in conjunction with Pacific La Nina events. The IOD leads many hydro-climate variables by three months and offers predictability for low flows during the northeast monsoon.

Rising maximum temperatures and diurnal winds tend to stimulate runoff on the western flank of the Rwenzori Mountains, which feeds into the Congo Basin. Divergent easterly winds induce sinking motions that lead to fast warming of mountain tops. The CNRM6 projection for rainfall from 1980 to 2050 shows a gradual upward trend interspersed with intense dry spells, highlighting key elements of a changing climate that may require restoration of catchment landscapes and channelization of runoff to limit the impacts of flash-floods and drought. Using global data assimilation products increases the transferability of methods beyond this case. But gaps in scientific understanding remain that require validation with local data to improve confidence in the application of engineering solutions.

Author Statement

The author Prof. Mark R. Jury performed all the conceptualization, analysis and interpretation of this research.

Declaration of Competing Interest

The authors declare that they have no known competing financial interests or personal relationships that could have appeared to influence the work reported in this paper.

Data Availability

Data will be made available on request.

Acknowledgements

Data were analyzed from the KNMI Climate Explorer, IRI Climate Library, NASA giovanni, NOAA Ready ARL, and Colorado State Cloudsat websites. This work contributes to the Acer-Africa assessment of Mobuku River hydropower resources, in collaboration with Dr B Rawlins of Univ Zululand. The author acknowledges support from the South African Dept of Higher Education and Puerto Rico Climate Office. A data spreadsheet is available on request.

Appendix

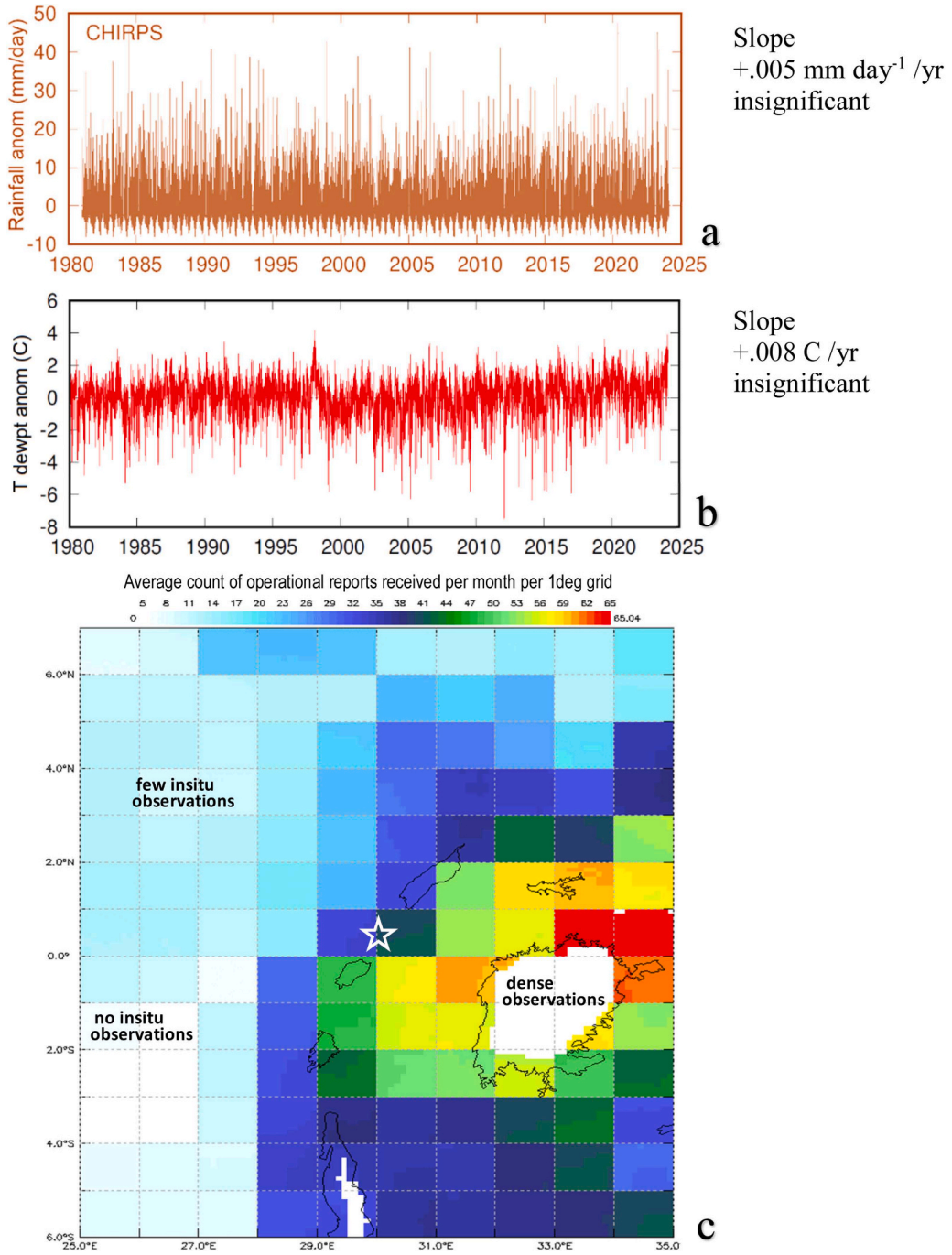

Fig A1. a,b) Daily anomalies of rainfall and dewpoint temperature in the catchment area 0.25–0.4 N, 29.85–30.1E. The upper graph is the basis for Fig. 3b, the lower graph is Fig. 2d,e. c) Station reporting density (month^{-1} /1°grid) clustered around Lake Victoria; reports from the Congo are nearly absent 2000–2021.

References

Berkley Energy, 2023. Updated hydrological assessment of Uganda's hydro portfolio, Arup UK ltd, report 292641, 40 pp.
Byakatonda, J., Openy, G., Sempewo, J.I., Mucunguzi, D.B., 2021. Over a century evidence of historical and recent dryness/wetness in sub-humid areas of Uganda, East Africa. Meteorol. Appl. 28, e2028.

Clarke, H., Nolan, R.H., DeDios, V.R., et al., 2022. Forest fire threatens global carbon sinks and population centres under rising atmospheric water demand. Nat. Commun. 13, 7161.
Cook, K.H., Vizy, E.K., 2019. Contemporary climate change of the African monsoon systems. Curr. Clim. Change Rep. 5, 145–159.
Finney, D.L., Marsham, J.H., Walker, D.P., et al., 2020. The effect of westerlies on East African rainfall and the associated role of tropical cyclones and the Madden–Julian Oscillation. Q. J. R. Meteorol. Soc. 146, 647–664.
Funk, C.C., Peterson, P.J., Landsfeld, M.F., et al., 2014. A quasi-global precipitation time series for drought monitoring. US Geological Survey. Data 832, doi. Org. /110. 3133/ds8 32.
Gelaro, R., McCarty, W., Suárez, M.J., et al., 2017. The modern-era retrospective analysis for research and applications v2 (MERRA2). J. Clim. 30, 5419–5454.
Harrigan, S., Zsoter, E., Alfieri, L., et al., 2020. GloFAS-ERA5 operational global river discharge reanalysis 1979–present. Earth Syst. Sci. Data 12, 2043–2060.
Herrnegger, M., Stecher, G., Schwatke, C., Olang, L., 2021. Hydroclimatic analysis of rising water levels in the great Rift Valley lakes of Kenya. J. Hydrol. Reg. Stud. 36, 100857.
Hersbach, H., Bell, B., Berrisford, P., et al., 2020. The ERA5 global reanalysis. Q. J. R. Meteorol. Soc. 146, 1999–2049.
Hogan, E., Shelly, A., Xavier, P., 2015. The observed and modelled influence of the Madden–Julian Oscillation on east African rainfall. Meteorol. Appl. 22, 459–469.
Hou, A.Y., Kakar, R.K., Neeck, S., et al., 2014. The global precipitation measurement mission. Bull. Am. Meteorol. Soc. 95, 701–722.
IPCC, 2021. Climate Change: The Physical Science Basis, contribution of WG-I to AR6, Intergovernmental Panel on Climate Change. Masson-Delmotte V, Zhai P, Pirani A, et al. (eds) Cambridge Univ Press, UK, 2391 pp.
Jury, M.R., 2017b. Warm spells on the East African plateau and impacts in the White Nile basin. Theor. Appl. Climatol. 129 https://doi.org/10.1007/s00704-017-2195-5.
Jury, M.R., 2017a. Uganda rainfall variability and prediction. Theor. Appl. Climatol. 128 https://doi.org/10.1007/s00704-017-2135-4.
Jury, M.R., 2018. South Indian ocean rossby waves. Atmos. Ocean 56, 322–331.
Jury, M.R., Whitehall, K., 2010. Warming of an elevated layer over Africa. Clim. Change 99, 229–245.
Karlsson, K.G., et al., 2020 CLARA-CM-SAF cloud, albedo & surface radiation dataset from AVHRR data v2.1, ESA satellite application facility for climate monitoring, doi10.5676/.
Lee, H.T., Gruber, A., Ellingson, R.G., et al., 2007. Development of the HIRS outgoing longwave radiation climate dataset. J. Atmos. Ocean. Technol. 24, 2029–2047.
MacKay, A.W., Lee, R., Russell, J.M., 2021. Recent climate-driven ecological changes in tropical montane lakes of Rwenzori Mountains National Park in central Africa. J. Paleolimnol. 65, 219–234.
MacLeod, D., Kolstad, E.W., Michaelides, K., Singer, M.B., 2024. Sensitivity of rainfall extremes to unprecedented Indian Ocean Dipole events. Geophys. Res. Lett. 51 e2023GL105258.
Munday, C., Washington, R., 2018. Systematic climate model rainfall biases over southern Africa: links to moisture circulation and topography. J. Clim. 31, 7533–7548.
Nicholson, S.E., 2018. The ITCZ and the seasonal cycle over equatorial Africa. Bull. Am. Meteorol. Soc. 99, 337–348.
Nsubuga, F., Namutebi, E., Nsubuga-Senfuma, M., 2014. Water resources of Uganda: an assessment and review. J. Water Resour. Prot. 6, 1297–1315.
Palmer, P.I., Wainwright, C.M., Dong, B., et al., 2023. Drivers and impacts of Eastern African rainfall variability. Nat. Rev. Earth Environ. 4, 254–270.
Pepin, N., Bradley, R.S., Diaz, H.F., et al., 2015. Elevation-dependent warming in mountain regions of the world. Nat. Clim. Change 5, 424–430.
Pielke, R.A. & Segal, M., 1986. Mesoscale circulations forced by differential terrain heating. Mesoscale Meteorology and Forecasting, Ray P (ed), AMS, 516-548.
Pinzon, J.E., Tucker, C.J., 2014. A non-stationary AVHRR NDVI time series. Remote Sens. 6, 6929–6960.
Prinz, R., Heller, A., Ladner, M., Nicholson, L., Kaser, G., 2018. Mapping the loss of Mt. Kenya's glaciers: an example of the challenges of satellite monitoring of very small glaciers. Geosciences 8, 174.
Raghavendra, A., Xia, G., Zhou, L., Jiang, Y., 2022. Orographic enhancement of rainfall over the Congo Basin. Atmos. Sci. Lett. 23, e1079.
Roy, I., Mliwa, M., Troccoli, A., 2024. Important drivers of East African monsoon variability and improving rainy season onset prediction. Nat. Hazards 120, 429–445.
Tanelli, S., Durden, S.L., Im, E., et al., 2008. CloudSat's cloud profiling radar after two years in orbit: performance, calibration, and processing. IEEE Trans. Geosci. Remote Sens. 46, 3560–3573.
Taylor, R.G., Mileham, L., Tindimugaya, C., Mwebembezi, L., 2009. Recent glacial recession and its impact on alpine riverflow in the Rwenzori Mountains of Uganda. J. Afr. Earth Sci. 55, 205–213.
Thompson, L.G., Mosley-Thompson, E., Brecher, H., et al., 2006. About tropical climate change: past and present. Proc. Natl. Acad. Sci. 103, 10536–10543.
UNDP, 2013. A study of flooding in the Rwenzori Mountains for effective disaster risk management. U. Nations Dev. Program. Rep. 36.
Voldoire, A., Saint-Martin, D., Senesi, S., et al., 2019. Evaluation of CMIP6 experiments with CNRM-CM6. J. Adv. Model. Earth Syst. 11, 2177–2213.
Wainwright, C.M., Marsham, J.H., Keane, R.J., et al., 2019. 'East African Paradox' rainfall decline due to shorter not less intense long rains. Climatol. Atmosp. Sci. 2, 1–9.
Yang, W., Seager, R., Cane, M.A., Lyon, B., 2015. The annual cycle of east African precipitation. J. Clim. 28, 2385–2404.